Thin Solid Films 570 (2014) 371–375

Contents lists available at ScienceDirect

Thin Solid Films

journal homepage: www.elsevier.com/locate/tsf

Correlation between palladium chemical state and photocatalytic performance of TiO_2–Pd based nanoparticles

Ming-Chung Wu [a,*], I-Chun Chang [a], Wei-Kang Huang [a], Yu-Chieh Tu [b], Che-Pu Hsu [b], Wei-Fang Su [b]

[a] Department of Chemical and Materials Engineering, College of Engineering, Chang Gung University, Taoyuan 33302, Taiwan
[b] Department of Materials Science and Engineering, National Taiwan University, Taipei 10617, Taiwan

ARTICLE INFO

Available online 18 April 2014

Keywords:
TiO_2
Photocatalyst
Photocatalytic hydrogen production
Photodegradation
X-ray photoelectron spectroscopy

ABSTRACT

Photocatalytic processes can be used to illustrate both solar energy conversion and environmental friendly applications. In this study, we synthesize several titanium dioxide–palladium (TiO_2–Pd) based catalysts by wet impregnation method plus hydrogen-thermal reduction process in order to develop high-effective photocatalysts that can be easily produced even in industrial quantities. Moreover, we examine the effects of hydrogen-thermal reduction process on the photocatalytic performance of TiO_2–Pd based catalysts. From X-ray photoelectron spectroscopy analysis, increasing the hydrogen reduction process time results in the decreasing of palladium ion (Pd^{2+}) and palladium oxide (PdO), but it causes the increasing of palladium (Pd) metal. The hydrogen reduction process is helpful for the preparation of TiO_2–Pd based catalysts with high photocatalytic decomposition of organic dyes (the apparent reaction rate constant ~0.124 min^{-1} under solar simulator irradiation) and excellent photocatalytic hydrogen production rate (~26,000 μmol/g·h under UV-B irradiation). The TiO_2–Pd based catalysts prepared in this study exhibit high photocatalytic performance. They are also industrially relevant especially when the low cost of Pd metal is taken into consideration.

1. Introduction

Photocatalytic processes have been used to demonstrate several aspects of renewable energy production and the decomposition of organic pollutants in recent years [1,2]. Titanium dioxide (TiO_2) is probably the most favorable photocatalyst due to its environmental friendly nature, low cost, and high photocatalytic activity. It has shown excellent photostability as demonstrated in photocatalytic production of hydrogen [3–5], in working electrodes of dye-sensitive solar cells [6], in antimicrobial surface coatings [7] and in decomposition of volatile organic compounds from the air [8]. Among various TiO_2 photocatalysts, Degussa P25 (which consists of 70% anatase with a minor amount of rutile and a small amount of amorphous phase [9,10]) is widely used because of its relatively high level of activity in many photocatalytic reaction systems. Actually, it is not easy to find a photocatalyst showing activity higher than that of Degussa P25. Therefore, it has been used as a standard TiO_2 photocatalyst. Photocatalytic reactions of Degussa P25 have been reported in thousands of papers since 1990. Schottky interface is a potential energy barrier for electrons formed among metal nanoparticles with a large work function and n-type TiO_2, while p-type semiconductors in contact with TiO_2 result in p–n junctions at the potential energy barrier [11]. Since p–n junctions exhibit rectifying electrical transport behaviors, an efficient charge separation of the photogenerated electron–hole pairs is achieved, preventing the undesired electron–hole recombination. According to several studies, decorations of TiO_2 with metals and metal oxides such as platinum (Pt) [12–14], gold (Au) [12,15], palladium (Pd) [16], palladium oxide (PdO) [16], nickel (Ni) [17], and silver (Ag) [18] have been found to enhance the photocatalytic performance. Similar effects can be obtained by using carbon nanotubes [19] and graphene [20]. However, to decorate TiO_2 catalysts with noble metal is also an effective method to obtain the catalysts with high photocatalytic activity. Moreover, some literatures reported metal nanoparticles (NPs) such as Au, Ag, and copper (Cu) could absorb and scatter visible light due to localized surface plasmon resonance (LSPR). LSPR can produce the photopotential and photocurrent responses depended on the size, shape, surface state, surrounding environment, metal features, etc. [21–23].

In order to develop a catalyst with high photocatalytic activity, Ismail et al. reported a synthesis of mesoporous PdO–TiO_2 nanocomposites with different PdO concentrations through simple one-step sol–gel reactions. Pd^{2+}-ions were immobilized into TiO_2 networks by cross linking triblock copolymer, the structure-directing agents, to develop highly efficient PdO–TiO_2 photocatalyst. The measured photonic efficiency was as high as 19.5% [24]. Moreover, Roy et al. reported a synthesis of $Ti_{1-x}Pd_xO_{2-\delta}$ crystallization in anatase phase with Pd^{2+}-ion, showing that enhanced carbon monoxide (CO) oxidation at Pd^{2+}-ion site. Oxygen (O_2) or nitrogen monoxide (NO) photo dissociation at oxide ion vacancy is responsible for the enhanced catalytic activity [25]. With more advantages, Pd is the cheapest and most commonly used

* Corresponding author.
E-mail address: mingchungwu@mail.cgu.edu.tw (M.-C. Wu).

http://dx.doi.org/10.1016/j.tsf.2014.04.026
0040-6090/

metal among the noble metals for co-catalyst with TiO_2 photocatalyst. The cost of Pd metal is approximately 20%–25% of that of Pt metal [26].

Herein, we synthesized several TiO_2–Pd based catalysts by wet impregnation method, followed by hydrogen-thermal reduction process in order to develop high effective photocatalyst that can be easily produced in industrial quantities. The chemical state of Pd-based nanoparticles decorated on TiO_2 photocatalyst surface is controlled by changing the time of the hydrogen-thermal reduction process. The chemical state and morphology of the Pd-based nanoparticles can be determined by X-ray photoelectron spectroscopy (XPS) and transmission electron microscopy (TEM). Moreover, the photodegradation performance of organic dyes and photocatalytic production of hydrogen for TiO_2–Pd based catalysts are also measured in this study.

2. Experimental details

For the preparation of TiO_2–Pd based catalysts, 29.2 mg of palladium(II) acetylacetonate ($Pd(C_5H_7O_2)_2$, Aldrich, 99%) was dissolved in 200 mL of acetone to helped suspend 1.00 g TiO_2 nanoparticle (Degussa P25). This is followed by ultrasonic agitation for 3 h and stirred for 6 h. After this, the samples were calcined in the air at 300 °C for 2 h, and then reduced in 15% H_2 (in Ar buffer) flow at 500 °C for 0, 15, 60, 240 and 960 min to obtain the products. The products were given the following names respectively, TiO_2–Pd000, TiO_2–Pd015, TiO_2–Pd060, TiO_2–Pd240 and TiO_2–Pd960 with ~1.0 wt.% Pd metal loading.

The surface structure/morphology and crystalline structure of TiO_2 nanoparticles (Degussa P25) and TiO_2 decorated with Pd-based nanoparticles (TiO_2–Pd000, TiO_2–Pd015, TiO_2–Pd060, TiO_2–Pd240 and TiO_2–Pd960) were studied by TEM (EFTEM, LEO 912 OMEGA, 120 kV). XPS (Kratos Axis Ultra, mono Al Kα X-ray source, analysis area of 5 × 5 mm^2, applying charge neutralizer) was used to study the chemical composition as well as the chemical state of the Pd anchored on the TiO_2 nanoparticles.

For the quantification of the photodegradation of methylene blue, 20.0 mg of catalyst was sonicated for 2 min in 50 mL of 10 mg/L methylene blue (Arcos, $C_{16}H_{18}ClN_3S \cdot H_2O$, >96+%) aqueous solution. The suspension was irradiated with solar simulator (Newport, 92193, 6 in. by 6 in., 100 mW/cm^2) under vigorous stirring at ambient condition. After centrifuging for 15 min at 5000 rpm, the UV–vis spectrum (Perkin-Elmer UV Instrument: Lambda 35) of the remained methylene blue in the supernatant was recorded to be in the 300 to 900 nm wavelength range. The concentrations of the methylene blue was calculated from the absorbance at $\lambda = 662$ nm, extrapolated from a previously plotted calibration curve.

Photocatalytic hydrogen generation tests were carried out by using 1:1 volume ratio mixture of ethanol and water (total 2.0 L) in which 10.0 mg of TiO_2-based catalyst was suspended prior to each experimental condition. The temperature of the mixture was kept near room temperature. For light source, six pieces of UV-B lamps (Sankyo Denki G15T8E UV-B lamps, the wavelength of maximum emission of UV-B lamp was ~312 nm, and the power was 8.0 W) were placed in a hexagonal arrangement around the reactor. The distance between each lamp and reactor is about 5.0 cm as shown in Fig. 1. To avoid sedimentation of the catalyst powders, nitrogen (99.995%) was bubbled through the reactor with a flow rate of 400 mL/min, serving also as a purging gas for the evolving gaseous products. The outlet of the reactor was connected to a cold trap, a molecular sieve, and a hydrogen analyzer (Status Scientific Controls Ltd, FGD3).

3. Results and discussion

TEM images of TiO_2 decorated with Pd-based nanoparticles (TiO_2–Pd240) are shown in Fig. 2(a, b). TiO_2 catalyst in this study is a commercial product, Degussa P25, to be a common standard for comparing with TiO_2–Pd based catalysts. Degussa P25's size ranges from 25 to 45 nm. Pd-based nanoparticles distributed on the surface of TiO_2 catalyst presented uniform size distribution with average particle diameters of 4.2 ± 0.7 nm as shown in the inset of Fig. 2(c).

Fig. 3 shows the normalized absorption spectra of TiO_2 catalysts (Degussa P25) and TiO_2–Pd based catalysts (TiO_2–Pd000, TiO_2–Pd015, TiO_2–Pd060, TiO_2–Pd240 and TiO_2–Pd960). The absorption spectra show that the TiO_2–Pd based catalysts have higher absorptivity than that of the pure TiO_2 catalyst. Moreover, the absorption spectra of various TiO_2–Pd based catalysts exhibit similar absorption behaviors. Fig. 3 reveals that the TiO_2–Pd based catalysts treated with different lengths of hydrogen-thermal reduction time have no obvious absorption variation.

For XPS examination, we measured the Pd-based signals, such as Pd, PdO, and Pd^{2+}, between 333 to 338.5 eV of binding energy. TiO_2–Pd based catalysts in this study show the appearance of different chemical states of Pd $3d_{5/2}$ as shown in Fig. 4(a). For XPS analysis, the full-width half-maximum (FWHM) of each fitted peaks was kept constant of 1.1 eV by XPS peak 41. According to XPS spectra, TiO_2–Pd000 displays the main presence of Pd^{2+}-ion and PdO. The components with higher binding energies around ~335.2 eV and ~336.7 eV are corresponding to PdO and Pd^{2+}-ion respectively. The chemical states of the Pd-based nanoparticles changed from Pd^{2+}-ion and PdO to Pd as the reduction time increases at fixed calcination temperature of 500 °C. The percentage of total Pd amount for Pd, PdO and Pd^{2+}-ion of TiO_2–Pd based nanoparticles is shown in Fig. 4(b). For TiO_2–Pd240, the percentages of the total Pd amount for Pd and Pd^{2+}-ion are 42.1% and 6.1% respectively, but the amount of PdO is as high as 51.8%. Pd $3d_{5/2}$ component around 334.6 eV shows the presence of Pd metal on the surface of TiO_2 nanoparticles. Pd shows lower binding energy (Pd $3d_{5/2}$: 335.1 eV) of metallic state than previously reported [25]. This may be due to the size effect or the increased electron density on the metal nanoparticles from nanoparticle (active site)–support interaction.

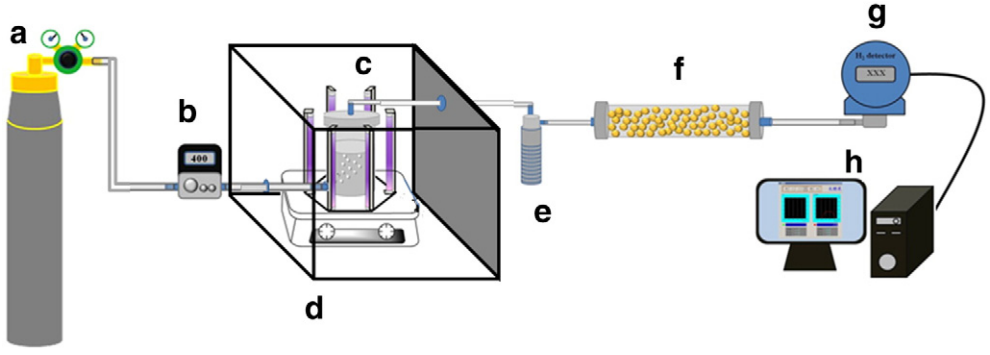

Fig. 1. The schematic illustration of our photocatalytic hydrogen generation measurement, including (a) nitrogen gas cylinder, (b) electronic flow meter, (c) quartz reactor, (d) light source, (e) Dewar flask, (f) molecular sieve, (g) hydrogen gas detector, and (h) data processing system.

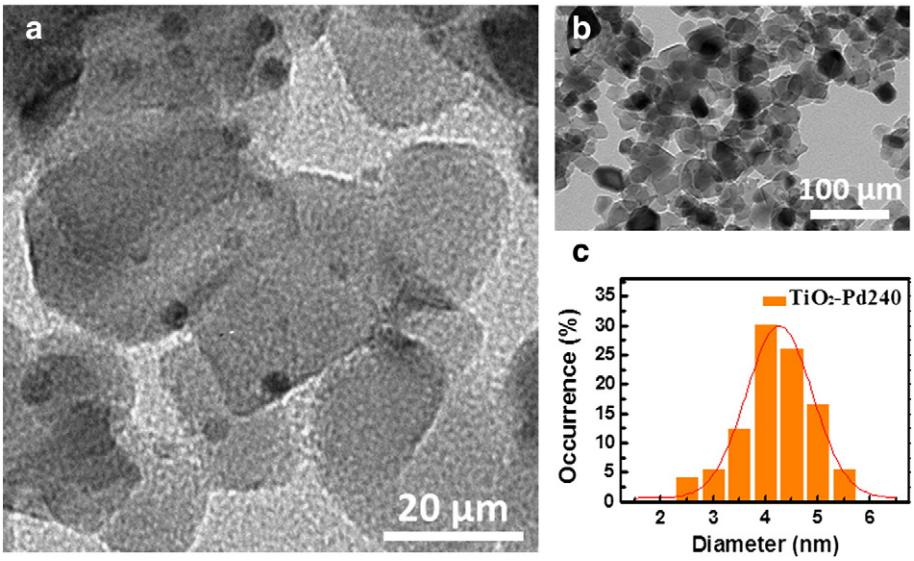

Fig. 2. (a, b) TEM images of TiO_2 catalysts decorated with Pd-based nanoparticles (TiO_2–Pd240), and (c) the corresponding Pd-based nanoparticle size distribution on TiO_2 catalysts.

Light-induced photodegradation of methylene blue in aqueous solution for pure TiO_2 catalyst (Degussa P25) and various TiO_2–Pd based catalysts (TiO_2–Pd000, TiO_2–Pd015, TiO_2–Pd060, TiO_2–Pd240 and TiO_2–Pd960) was tested using solar simulator, and each 20.0 mg catalyst was dispersed in 150 mL of solution. UV–vis spectra of methylene blue as a function of solar light irradiation time were recorded. From the absorbance measured at $\lambda = 662$ nm, the methylene blue concentration could be calculated using a calibration curve measured previously. The initial concentration of methylene blue is 20.0 mg/L, and the degradation percentage ($\boldsymbol{C/C_0}$) of methylene blue versus the irradiation time over pure TiO_2 catalyst and TiO_2–Pd based catalysts under the irradiation of solar simulator is shown in Fig. 5(a). The process of TiO_2-based catalysts catalyzing photodegradation of methylene blue essentially follows Langmuir–Hinshelwood kinetics, which can be simplified to the apparent first-order kinetics at lower initial methylene blue concentrations. This can be mathematically described as $\boldsymbol{\ln(C_0/C) = kt}$, where $\boldsymbol{C}$ is the concentration of the dye at time $\boldsymbol{t}$, $\boldsymbol{C_0}$ is the initial concentration, and $\boldsymbol{k}$ is the apparent reaction rate constant. Plotting the logarithm of the reciprocal of the measured methylene blue concentration as a function of time, we obtain linear slopes for each catalyst studied, which agreed with the Langmuir–Hinshelwood mode. The apparent reaction rate constants for the photodegradation of methylene blue over various catalysts are shown in Table 1. Among the TiO_2–Pd based catalysts, TiO_2–Pd240 exhibits the highest apparent reaction rate constant and TiO_2–Pd000 shows the lowest apparent reaction rate constant. Fig. 5(b) shows UV–vis absorbance spectra of methylene blue as a function of illumination time with TiO_2–Pd240 catalyst. When the hydrogen-thermal reduction time is more than 240 min at the fixed reduction temperature of 500 °C, the reaction rate constant is approaching the highest value obtained. Hence, the hydrogen-thermal reduction time of 240 min should be enough for preparing the TiO_2–Pd based catalyst with high photodegradation performance. From the results of the photodegradation tests and the XPS analysis, it was found that TiO_2–Pd based catalysts with high concentration of PdO are suitable for the applications of photodegradation of organic dyes. Additionally, the electric fields localized around Pd-based nanoparticles by surface plasmon resonance could be used as light-harvesting antennae for photocurrent enhancement. The plasmon-induced charge separation at interfaces between Pd-based nanoparticles and TiO_2 could be an apparent effect [24]. Therefore, the chemical state of palladium plays an important role for the preparation of TiO_2–Pd based catalysts with high photocatalytic activity.

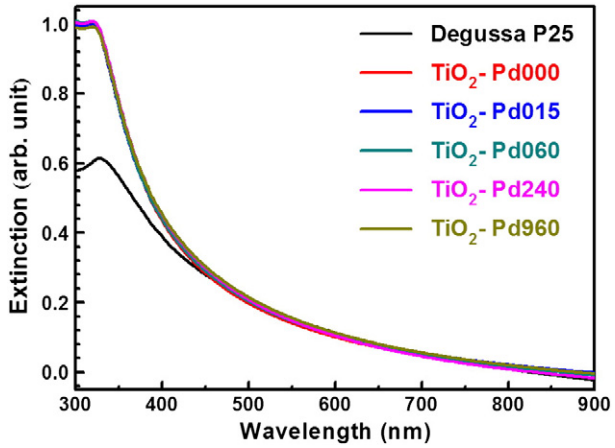

Fig. 3. Absorption spectra of TiO_2 catalysts and TiO_2–Pd based catalysts.

Photocatalytic hydrogen production tests of various TiO_2-based catalysts under UV-B irradiation were measured in our study and the photocatalytic hydrogen production rates were shown in Table 1. For the pure TiO_2, it is not active in the photocatalytic production of hydrogen, and must be combined with a precious transition metal to yield an active photocatalyst. Among the TiO_2–Pd based catalysts, TiO_2–Pd060 and TiO_2–Pd240 exhibit the high photocatalytic hydrogen production rate. When the thermal-hydrogen reduction time is more than 60 min, the photocatalytic hydrogen production rate also approaches the highest value from Table 1. It is clearly seen that the chemical state of palladium influences the rate of photocatalytic production of hydrogen. The purpose of Pd-based nanoparticle decorated on TiO_2 surface is to generate a Schottky barrier at the interface between TiO_2 and Pd-based nanoparticles. The highest hydrogen production rate is found with TiO_2–Pd240. Its hydrogen production rate is as high as 260 μmol/h for 10.0 mg catalyst. Moreover, from the results of XPS study as shown in Fig. 4, the amount of Pd metal in Pd-based nanoparticles increases as reduction time increases. The chemical state of Pd-based nanoparticles decorated on TiO_2 surface plays an important role for photocatalytic production of hydrogen. Pd-based nanoparticle decorations with the appropriate chemical states on TiO_2 surface could capture the photogenerated electrons effectively and could reduce the rate of electron–hole recombination to enhance the photocatalytic hydrogen production rate. However, the photocatalytic activities of the TiO_2-

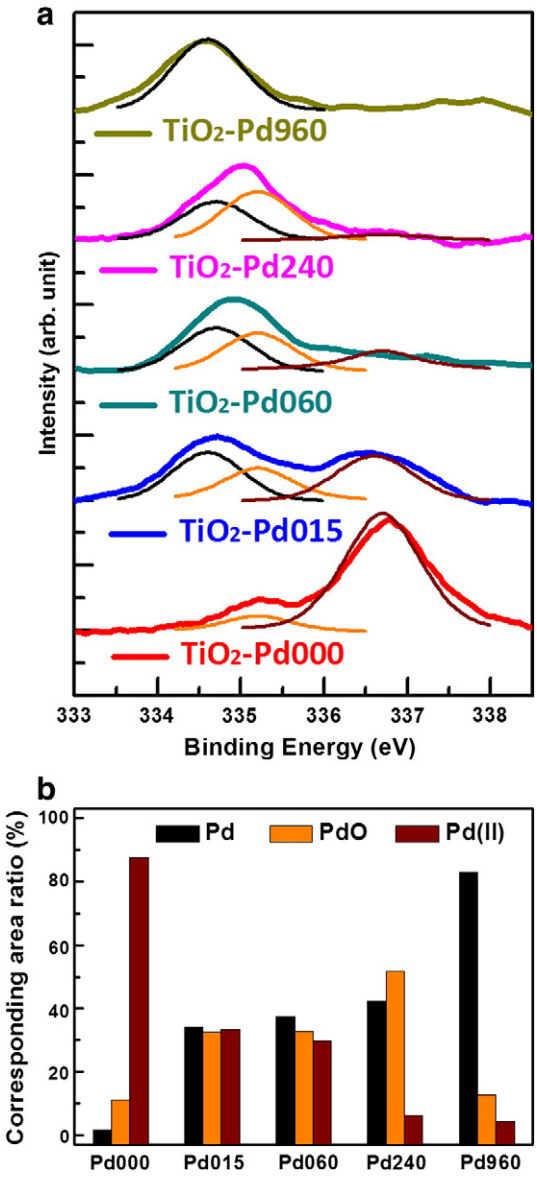

Fig. 4. (a) XPS Pd $3d_{5/2}$ spectra of various TiO_2–Pd based catalysts, and (b) the percentage of total Pd amount for Pd, PdO, and Pd^{2+}-ion of TiO_2–Pd based catalysts.

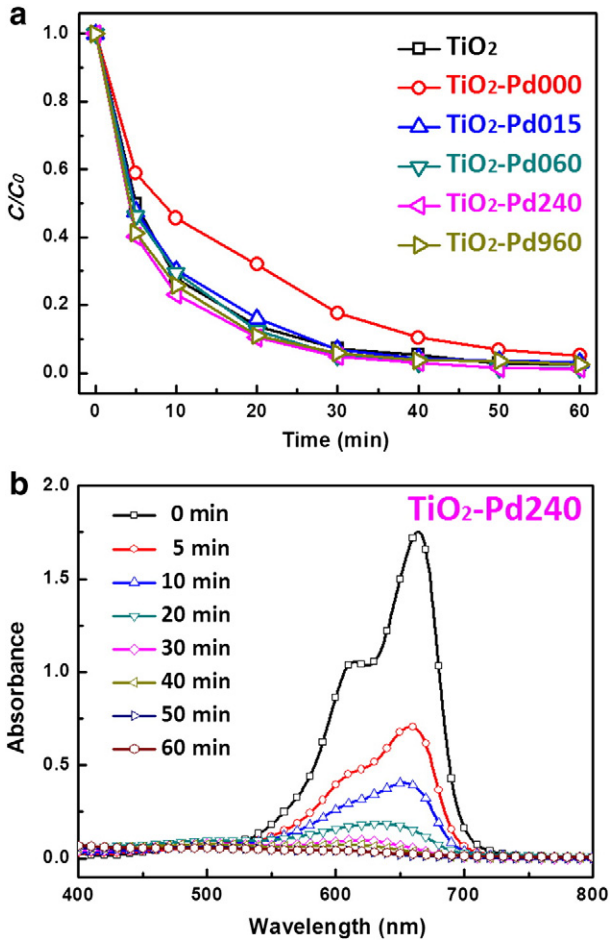

Fig. 5. (a) Plot of the degradation percentage (C/C_0) of methylene blue versus the irradiation time over pure TiO_2 catalyst and TiO_2–Pd based catalysts under the irradiation of solar simulator, and (b) UV–vis absorbance spectra of methylene blue (initial concentration of 20.0 mg/L) as a function of illumination time with TiO_2–Pd240 catalyst (20.0 mg dispersed in 150 mL of solution).

based materials in the two different kinds of reactions do not show similar results. Popov group reported the different activities of a set of photocatalytic materials in different reactions recently. They concluded that generalization of photocatalytic activity of semiconducting nanomaterials based on a single test molecule/microbe is not always appropriate, 7as a number of different factors can influence the behaviors [27].

4. Conclusion

This study examines the effect of hydrogen-thermal reduction process time on TiO_2–Pd based catalysts for the performance of photocatalytic decomposition of organic dyes and photocatalytic production of hydrogen. Based on XPS study, as the reduction time increases, the amount of Pd metal in Pd-based nanoparticles increases, but the amount of Pd^{2+}-ion decreases. The hydrogen-thermal reduction process is suitable for the preparation of TiO_2–Pd based catalysts, because it produces catalysts with excellent ability of photocatalytic decomposition of organic dyes and high photocatalytic hydrogen production rate. TiO_2–Pd based catalysts exhibit industrially relevant interests due to the low cost (approximately 20%–25% of that of Pt metal) and high photocatalytic activity. The highest photocatalytic hydrogen production rate found with TiO_2–Pd240 is as high as 26,000 μmol/g·h under UV-B irradiation.

Acknowledgment

Financial support obtained from the Ministry of Science and Technology of Taiwan and Chang Gung University Research Project is highly appreciated. We appreciate Dr. Andrey Shchukarev and Prof. Jyri-Pekka Mikkola at Umeå University of Sweden, Prof. Kordas at University of Oulu of Finland, and Dr. Ming-Tao Lee group (BL-13A1) at National

Table 1
The apparent reaction rate constants for the photodegradation of methylene blue and photocatalytic hydrogen production rates of various TiO_2-based nanoparticles.

Sample	k (min^{-1})	Hydrogen production rate (μmol/h)
TiO_2	0.107	0
TiO_2–Pd000	0.052	211
TiO_2–Pd015	0.100	220
TiO_2–Pd060	0.109	258
TiO_2–Pd240	0.124	260
TiO_2–Pd960	0.121	239

Synchrotron Radiation Research Center of Taiwan for useful discussions and suggestions of XPS analysis and crystalline structure.

References

[1] B.S. Boroujeny, A. Afshar, A. Dolati, Photoactive and self-cleaning TiO_2–SiO_2 thin films on 316L stainless steel, Thin Solid Films 520 (2012) 6355.

[2] K. Sridharan, E. Jang, T.J. Park, Novel visible light active graphitic C_3N_4–TiO_2 composite photocatalyst: synergistic synthesis, growth and photocatalytic treatment of hazardous pollutants, Appl. Catal. B Environ. 142–143 (2013) 718.

[3] J. Wang, P. Zhang, X. Li, J. Zhu, H. Li, Synchronical pollutant degradation and H_2 production on a Ti^{3+}-doped TiO_2 visible photocatalyst with dominant (0 0 1) facets, Appl. Catal. B Environ. 134–135 (2013) 198.

[4] M. Altomare, M. Pozzi, M. Allieta, L.G. Bettini, E. Selli, H_2 and O_2 photocatalytic production on TiO_2 nanotube arrays, Appl. Catal. B Environ. 136–137 (2013) 81.

[5] A. Kudo, Y. Miseki, Heterogeneous photocatalyst materials for water splitting, Chem. Soc. Rev. 38 (2009) 253.

[6] J. Burschka, N. Pellet, S.J. Moon, R. Humphry-Baker, P. Gao, M.K. Nazeeruddin, M. Gratzel, Sequential deposition as a route to high-performance perovskite-sensitized solar cells, Nature 499 (2013) 316.

[7] M.R. Hoffmann, S.T. Martin, W. Choi, D.W. Bahnemannt, Environmental applications of semiconductor photocatalysis, Chem. Rev. 95 (1995) 69.

[8] S. Horikoshi, S. Sakamoto, N. Serpone, Formation and efficacy of TiO_2/AC composites prepared under microwave irradiation in the photoinduced transformation of the 2-propanol VOC pollutant in air, Appl. Catal. B Environ. 140–141 (2013) 646.

[9] B. Ohtani, O.O. Prieto-Mahaney, D. Li, R. Abe, What is Degussa (Evonik) P25? Crystalline composition analysis, reconstruction from isolated pure particles and photocatalytic activity test, J. Photochem. Photobiol. A Chem. 216 (2010) 179.

[10] T. Ohno, K. Sarukawa, K. Tokieda, M. Matsumura, Morphology of a TiO_2 photocatalyst (Degussa, P-25) consisting of anatase and rutile crystalline phases, J. Catal. 203 (2001) 82.

[11] M.C. Wu, J. Hiltunen, A. Sapi, A. Avila, W. Larsson, H.C. Liao, M. Huuhtanen, G. Toth, A. Shchukarev, N. Laufer, A. Kukovecz, Z. Konya, J.P. Mikkola, R. Keiski, W.F. Su, Y.F. Chen, H. Jantunen, P.M. Ajayan, R. Vahtai, K. Kordas, Nitrogen-doped anatase nanofibers decorated with noble metal nanoparticles for photocatalytic production of hydrogen, ACS Nano 5 (2011) 5025.

[12] G.R. Bamwenda, S. Tsubota, T. Nalamura, M. Haruta, Photoassisted hydrogen production from water-ethanol solution: a comparison of activities of Au–TiO_2 and Pt–TiO_2, J. Photochem. Photobiol. A Chem. 89 (1995) 177.

[13] P. Wei, J. Liu, Z. Li, Effect of Pt loading and calcination temperature on the photocatalytic hydrogen production activity of TiO_2 microspheres, Ceram. Int. 39 (2013) 5387.

[14] G. Wu, T. Chen, X. Zong, H. Yan, G. Ma, X. Wang, Q. Xu, D. Wang, Z. Lei, C. Li, Suppressing CO formation by anion adsorption and Pt deposition on TiO_2 in H_2 production from photocatalytic reforming of methanol, J. Catal. 253 (2008) 225.

[15] O. Rosseeler, M.V. Shankar, M.K.L. Du, L. Schmidlin, N. Keller, V. Keller, Solar light photocatalytic hydrogen production from water over Pt and Au/TiO^2 (anatase/rutile) photocatalysts: influence of noble metal and porogen promotion, J. Catal. 269 (2010) 179.

[16] Q. Li, Y.W. Li, P. Wu, R. Xie, J.K. Shang, Palladium oxide nanoparticles on nitrogen-doped titanium oxide: accelerated photocatalytic disinfection and post-illumination catalytic "memory", Adv. Mater. 20 (2008) 3717.

[17] H.H. Tseng, M.C. Wei, S.F. Hsiung, C.W. Chiou, Degradation of xylene vapor over Ni-doped TiO_2 photocatalysts prepared by polyol-mediated synthesis, Chem. Eng. J. 150 (2009) 160.

[18] T. Hirakawa, P.V. Kamat, Charge separation and catalytic activity of Ag@TiO_2 core–shell composite clusters under UV-irradiation, J. Am. Chem. Soc. 127 (2005) 3928.

[19] K. Woan, G. Pyrgiotakis, W. Sigmund, Photocatalytic carbon-nanotube–TiO_2 composites, Adv. Mater. 21 (2009) 2233.

[20] H. Zhang, X. Lv, Y. Li, Y. Wang, J. Li, P25–graphene composite as a high performance photocatalyst, ACS Nano 4 (2010) 380.

[21] T. Yamaguchi, E. Kazuma, N. Sakai, T. Tatsuma, Photoelectrochemical responses from polymer-coated plasmonic copper nanoparticles on TiO_2, Chem. Lett. 41 (2012) 1340.

[22] M.C. Wu, Y. Chou, C.M. Chuang, C.P. Hsu, J.F. Lin, Y.F. Chen, W.F. Su, High-sensitivity Raman scattering substrate based on Au/$La_{0.7}Sr_{0.3}MnO_3$ periodic arrays, ACS Appl. Mater. Interfaces 1 (2009) 2484.

[23] J.H. Li, S.W. Chen, Y. Chou, M.C. Wu, C.H. Hsueh, W.F. Su, Effects of gold film morphology on surface plasmon resonance using periodic P3HT:PMMA/Au nanostructures on silicon substrate for surface-enhanced Raman scattering, J. Phys. Chem. C 115 (2011) 24045.

[24] A.A. Ismail, Mesoporous PdO–TiO_2 nanocomposites with enhanced photocatalytic activity, Appl. Catal. B Environ. 117 (118) (2012) 67.

[25] S. Roy, M.S. Hegde, N. Ravishaankar, G. Madras, Creation of redox adsorption sites by Pd^{2+} ion substitution in nanoTiO_2 for high photocatalytic activity of CO oxidation, NO reduction, and NO decomposition, J. Phys. Chem. C 111 (2007) 8153.

[26] M.C. Wu, A. Sapi, A. Avila, M. Szabo, J. Hiltunen, M. Huuhtanen, G. Toth, A. Kukovecz, Z. Konya, R. Keiski, W.F. Su, H. Jantunen, K. Kordas, Enhanced photocatalytic activity of TiO_2 nanofibers and their flexible composite films: decomposition of organic dyes and efficient H_2 generation from ethanol–water mixture, Nano Res. 4 (2011) 360.

[27] A. Sarkar, A. Shchukarev, A. Eino, K. Kordas, J.-P. Mikkola, P. Petrov, E. Tuchina, A. Popov, M. Darvin, M. Meinke, J. Lademann, V. Tuchin, Photocatalytic activity of TiO_2 nanoparticles: effect of thermal annealing under various gaseous atmospheres, Nanotechnology 23 (2012) 475711.